*magnetochemistry*

*Article*

# Dissolution of Lysozyme Amyloid Fibrils Using Magnetic Nanoparticles in an Alternating Magnetic Field: Design of an Effective Treatment for Cutaneous Amyloidosis

**Natália Andrýsková [1], Hana Vrbovská [2], Melánia Babincová [2], Peter Babinec [2,*] and Mária Šimaljaková [1]**

[1] Department of Dermatovenereology, Faculty of Medicine, Comenius University and Bratislava University Hospital, Mickiewiczova 13, 813 69 Bratislava, Slovakia
[2] Department of Nuclear Physics and Biophysics, Faculty of Mathematics, Physics and Informatics, Comenius University, Mlynská dolina F1, 842 48 Bratislava, Slovakia
* Correspondence: babinec@fmph.uniba.sk

**Abstract:** The purpose of this study was to apply functionalized magnetic nanoparticles for the treatment of amyloidosis, a disease characterized by the accumulation of aberrant protein forms with an insoluble amyloid structure. The dissolution and clearance of these extremely stable fibrils from lesions is very complicated. For this purpose, we examined the possibility of using magnetic nanoparticles that generate heat in an external alternating magnetic field with a frequency of 3.5 MHz. As a convenient model system, we used lysozyme fibrils. For the quantification of fibrillar status, we used Thioflavin T and Congo red, specific dyes which change their spectroscopic properties upon binding with the cross-beta structure of fibrils. We found that by using fluorescence, and polarization microscopy, as well as absorption spectrophotometry, the amyloid-like fibrils can be almost completely dissolved. The obtained results suggest that the application of magnetic nanoparticles could be a possible therapeutic intervention in cutaneous amyloidosis.

**Keywords:** lysozyme; magnetic nanoparticles; alternating magnetic field; cutaneous amyloidosis; hyperthermia

check for updates

**Citation:** Andrýsková, N.; Vrbovská, H.; Babincová, M.; Babinec, P.; Šimaljaková, M. Dissolution of Lysozyme Amyloid Fibrils Using Magnetic Nanoparticles in an Alternating Magnetic Field: Design of an Effective Treatment for Cutaneous Amyloidosis. *Magnetochemistry* **2023**, *9*, 84. https://doi.org/10.3390/magnetochemistry9030084

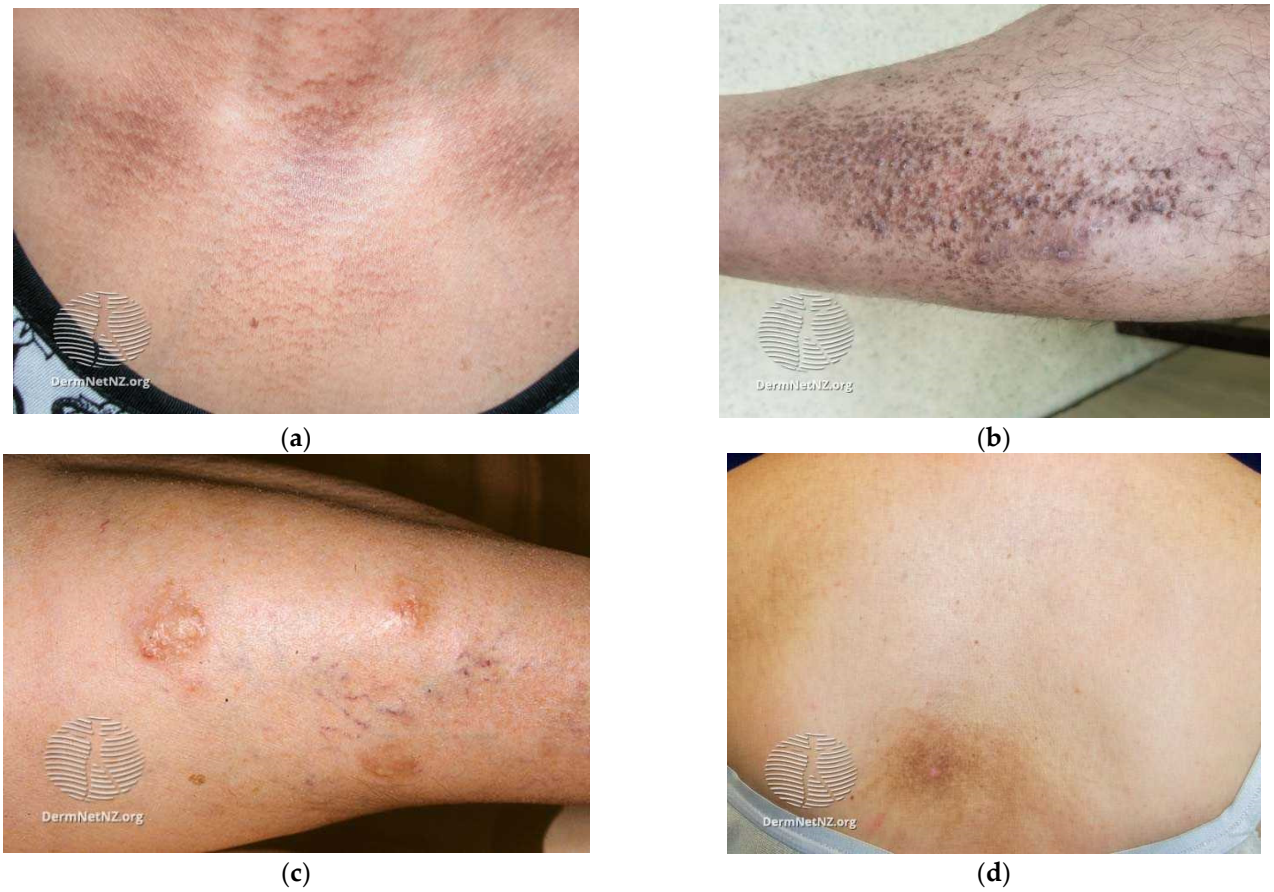
Academic Editor: Cristina Favieres

Received: 2 February 2023
Revised: 6 March 2023
Accepted: 14 March 2023
Published: 17 March 2023

**Copyright:** © 2023 by the authors. Licensee MDPI, Basel, Switzerland. This article is an open access article distributed under the terms and conditions of the Creative Commons Attribution (CC BY) license (https://creativecommons.org/licenses/by/4.0/).

## 1. Introduction

Amyloidosis is a class of diseases caused by the accumulation of normally soluble proteins, which, in this case, forms a beta sheet-rich structure that ultimately leads to cell death. Unfortunately, curative treatment is not available for these diseases [1]. Amyloidosis has a very long history, beginning in 1639 with Nicolaes Fonteyn describing a pathologically large human spleen full of white inclusions, which, in the year 1789, were named as amyloids by Antoine Portal. Nowadays, more than 100 human amyloid diseases are caused by fibrillar plaques [2–9]. The most known are Alzheimer's (Aβ peptides) and Parkinson's (α-synuclein) diseases. Less known diseases are, for example, familial amyloid polyneuropathy (transthyretin) and hemodialysis-related amyloidosis (β2-microglobulin). Despite the long history of these diseases, a detailed molecular mechanism of their origin is not completely known. Potential treatments become a compelling challenge and include inhibitors of molecules that induce fibril formation and fibril disaggregation [10–16]. The focus of this study is primary localized cutaneous amyloidosis, which is a rare chronic disorder characterized by the cutaneous deposition of insoluble amyloid protein between the dermis and epidermis in previously normal skin, without internal organ involvement [17–21]. There are three types: macular, nodular, and lichen (Figure 1). As therapeutic modes, topical and intralesional corticosteroids, capsaicin, DMSO, vitamin D3, colchicine, ultraviolet phototherapy in combination with psoralens, surgery, cryotherapy, and laser therapy are used [22–24].




(**a**) (**b**)

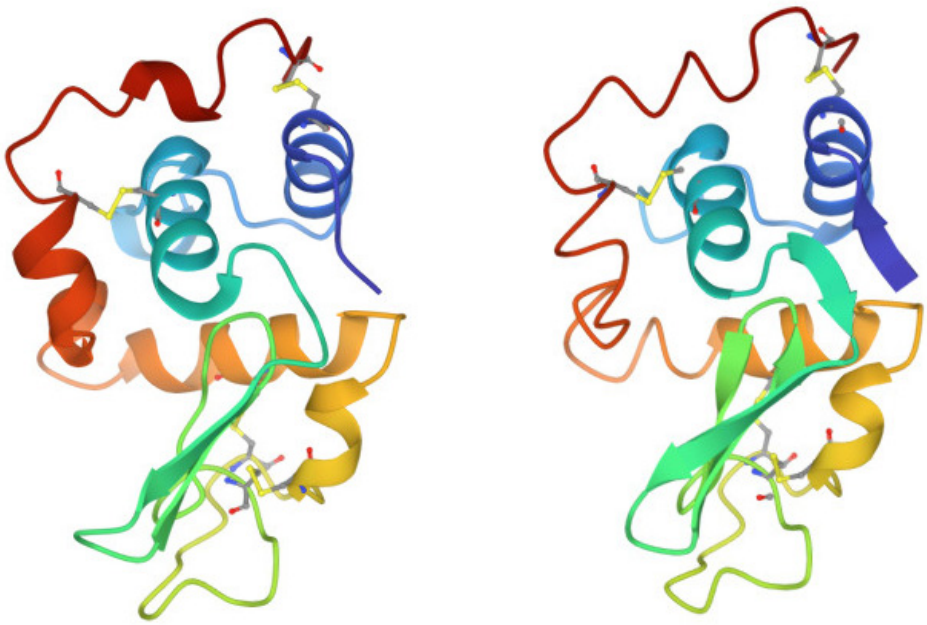
(**c**) (**d**)

**Figure 1.** Typical examples of primary localized cutaneous amyloidosis: (**a**) macular amyloidosis; (**b**) lichen amyloidosis; (**c**) nodular amyloidosis; (**d**) area of notalgia paraesthetica in macular amyloidosis. Available from dermnetnz.org (accessed on 13 February 2023), a free dermatology resource.

As a convenient protein, widely used for the study of amyloid formation, we used hen egg white lysozyme—HEWL. From a chemical aspect, lysozymes are glycoside hydrolases [25]. HEWL, with an almost identical tertiary structure to human lysozyme (Figure 2), is, therefore, a useful and easily available protein for the study of the process of amyloidosis. Although our goal is not directly the development of a method for removing lysozyme amyloid plaques, the method we are testing in this work may also be useful for this purpose [26,27].

Results from previous investigations revealed [29–33] that functionalized magnetic nanoparticles (MN) are also useful as an inhibitor of amyloidosis. Another emerging treatment, proved useful also in tumor eradication, is hyperthermia, efficient for the destruction of amyloid aggregates, for example, high-power ultrasound [34] microwaves [35,36] or laser treatment combined with gold nanoparticles [37,38]. The shortcoming of this approach is its diffuse nature and the need for long-time irradiation, which lead to unwanted side effects in adjacent tissues.

In this study we decided to evaluate the effect of heating MN after exposure to an alternating magnetic field (AMF) [39–46] on the dissolution of lysozyme fibrils. The leading idea is to investigate the possible synergism of hyperthermia and MN on their interaction with amyloid fibrils and on the enhancement of fibril dissolution. For these purposes, we utilized the unique properties of Congo red and Thioflavin T [47], which, after their specific binding to fibrils, can monitor the extent of HEWL fibrillation via spectroscopy, as well as fluorescence and polarization microscopy.



(**a**) (**b**)

**Figure 2.** Structures of (**a**) human lysozyme 1LOZ and (**b**) hen egg yolk lysozyme 1LYZ, available from the RSCB Protein Data Bank archive [28].

## 2. Materials and Methods

### *2.1. Materials*

HEWL, Congo red (CR), Thioflavin T (ThT), as well as other reagents were obtained from Sigma-Aldrich (St. Louis, MO, USA). Magnetic nanoparticles fluidMAG-OS, stabilized by the sodium salt of oleic acid with sodium carboxylate -$COO^-$ $Na^+$ functional group, were kindly supplied by Chemicell GmbH (Berlin, Germany). Buffered solutions were filtered through a 0.22 µm Micro Syringe filter (Millipore, Billerica, MA, USA).

### *2.2. Amyloid Fibrils Preparation*

For the preparation of stock solutions of fibrils, 20 mg·$mL^{-1}$ of HEWL was added to 100 mM phosphate buffer with 150 mM NaCl of pH 2 [47], which was then stored in an incubator at 65 °C for 7 days. As has been demonstrated, this is the most common condition used for inducing amyloid fibrillogenesis of HEWL. The experiments were carried out in such a way that the desired amounts of magnetic nanoparticles were added per 1 mL of fibrils with a concentration 2 mg·$L^{-1}$ (the molar extinction coefficient of HEWL is 37,646 $M^{-1}$ $cm^{-1}$ at 280 nm) and an AMF field with a frequency of 3.5 MHz was applied for 15 min.

### *2.3. Thioflavin T Binding Assays*

For fluorescence microscopy, 10 mM ThT (the molar extinction coefficient of ThT is 26,620 $M^{-1}$ $cm^{-1}$ at 412 nM) in double-distilled water was used. After binding ThT to the β-sheet-rich regions of fibrils, an approximately 10-fold fluorescence enhancement was observed at 482 nm, when excited at 450 nm.

### *2.4. Fluorescence Microscopy*

To 10 µL of fibrils deposited on a glass slide, 5 µL of 1 mM ThT was added, and the sample of amyloid fibrils was monitored by means of an epifluorescence unit of a Meiji Techno TC5400 (Saitmama, Japan) biological inversion microscope. Photos were acquired using a Canon EOS400-D camera (Figure 3).

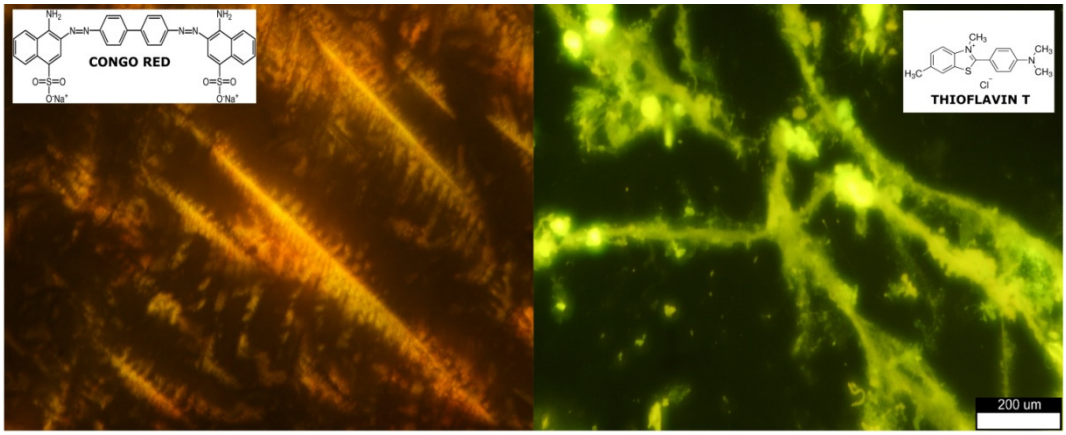



**Figure 3.** Visualization of amyloid structures using optical microscopy of CR-stained samples and polarized light between crossed polarizer and analyzer (**left**). ThT−stained samples were examined using fluorescence microscopy (**right**). Scale bar for both structures: 200 µm.

### *2.5. CR Binding Assay*

A CR dye solution in 25 mM phosphate buffer (pH 7.4) with a concentration of 25 µM (the molar extinction coefficient of CR is 45,000 $M^{-1}$ $cm^{-1}$ at 498 nm) was used, and 250 µL samples of HEWL fibrils, MN, and CR at desired concentrations were made. Spectral analysis was performed using a UV/Vis spectrophotometer UV mini-1240 (Shimadzu, Japan) in the range of 400 and 600 nm at room temperature using a quartz cuvette. CR staining is a standard method [48–51] for the visualization of amyloids, exhibiting apple-green birefringence under polarized light microscopy. The sample solution was deposited onto a glass slide after air-dried CR was added; when viewed under cross-polarized light, it exhibited a typical birefringence pattern (Figure 3).

### *2.6. Application of Alternating Magnetic Field (AMF)*

For the alternating magnetic field heating of MN bound to fibrils, we used an AMF generator GV6A (ZEZ, Rychnov, Czech Republic) working at 3.5 MHz (the magnetic field induction intensity was 1.2 $kAm^{-1}$). For cooling, water was circulated through the three 15 cm copper coil turns. The temperature was measured using a fiber-optic temperature sensor system (TS5 and FOTEMPMK-19, Optocon AG, Dresden, Germany).

### *2.7. Measurement of Magnetization Curve*

The magnetic properties were investigated using a MicroMagTM3900 (Princeton Measurements Corp., Westerville, OH, USA) vibrating sample magnetometer.

### *2.8. Calculation of Fractal Dimension*

For the determination of the fractal dimension of amyloid fibrils, the box-counting method was used, in which the surface profile was covered by N squares. By continuously changing the size of the squares r, their number N needed to cover the surface changes. In this way, we obtained data for the construction of the dependence $\log(N) = D \times \log(r)$. Its correlation is a straight line, the slope of which indicates the fractal dimension D of the given surface. Efficient and precise HarFA v. 5.5 software [52] was used for this purpose.

## 3. Results and Discussion

The magnetic nanoparticles have great potential in biomedical and clinical applications because of their unique physicochemical properties. Previous studies have reported that oleic acid and sodium oleate have a high affinity to the surface of iron oxide particles, being effective in the stabilization of nanoparticles by steric repulsion. It is possible to obtain iron oxide nanoparticles coated with monolayers of these surfactants, which are dispersible in organic solvents, or bilayers that can be dispersed in water. In the latter case,

the primary layer is first adsorbed onto the surface of the nanoparticles through chemical bonds between the carboxylic acid head groups of the surfactant molecules and the particle surface. The secondary layer is adsorbed onto the primary layer through hydrophobic interactions. Thus, the outermost layer provides hydrophilic groups that make the magnetic nanoparticles dispersible in aqueous solutions [53–56].

Toxicity is crucial for biomedical applications. Sun et al. [57] reported that magnetite nanoparticles coated with sodium oleate had a low toxicity and a better biocompatibility than magnetite nanoparticles coated with polyethylene glycol. Jain et al. evaluated the distribution, clearance, and biocompatibility of iron oxide magnetic nanoparticles coated with oleic acid and Pluronic® in rats [58]. They found that the coated nanoparticles did not cause long-term changes in liver enzyme levels, or induce oxidative stress, and, thus, can be safely used for drug delivery and imaging applications without significant levels of toxicity. For our experiments, we decided to use commercial sodium oleate-functionalized magnetic nanoparticles fluidMAG-OS. The advantage is that they are certified to "Good Manufacturing Process (GMP)" standards and may be more rapidly transferred to medically approval processes. Moreover, the toxicity and biocompatibility of these products must be resolved prior to their commercialization [58].

The magnetization of fluidMAG-OS, as shown in Figure 4, exhibits a value of about 41 emu/g at an external field strength of 15,000 A/m. This is approximately 44% of the bulk saturation magnetization of magnetite (92 emu/g). Furthermore, the magnetization does not saturate for this large value of the external field strength. Both results are signatures of small size superparamagnetic nanoparticle systems. The reduced value of magnetization may be partially attributed to dilution effects, caused by the presence of the sodium oleate adsorbed layer.

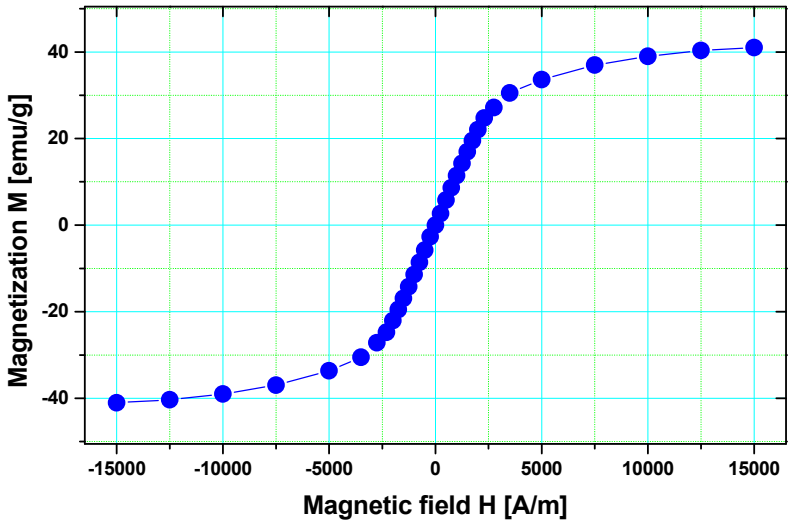



**Figure 4.** Magnetization curve of fluidMAG−OS magnetite nanoparticles; full symbols represent the experimental results, and the line represents the theoretical model.

From a patient safety aspect, it is important to realize that in the human body, water is a conductor, and eddy currents can be induced, causing a damaging effect by AMF. Therefore, there must be an upper limit for the allowed magnetic field and frequency that can be safely applied to living organisms. In 1984, Atkinson et al. [59] performed some clinical tolerance tests on healthy volunteers. They conducted the test using a single-turn induction coil, which was placed around the thorax of the volunteer. They also found that field intensities up to 35.8 A·turns/m at a frequency of 13.56 MHz could be thermally tolerated for extended periods of time. Importantly, for human exposure, it is pivotal to maintain the product of the magnetic field strength (H) and its frequency (f) below a threshold safety value known as the "Atkinson–Brezovich criterion", where the product of magnetic field intensity and frequency H × f should

not exceed $4.85 \times 10^9$ A/m/s. This criterion is considered, at best, an upper limit when applying a uniform field over an entire thorax of an adult. In practice, smaller coils are used with inhomogeneous fields and off-axis field directions, which are significantly different conditions than those used by Atkinson et al. [59]. These factors are expected to reduce eddy current heating. Hence, this criterion should not be considered as the only one. In a more recent study [60], the authors suggested that the upper limit for H × f should be 5 × 109 A/m/s. In this paper, H = $1.2 \times 10^3$ A/m and f = $3.5 \times 10^6$ $s^{-1}$ were used; therefore, our product was H × f = $4.2 \times 10^9$ A/m/s. Therefore, the AMF used in this study would also be safe for clinical applications.

An example of the heating curve of the fluidMAG-OS suspension is shown in Figure 5. For sodium oleate fluidMA-OS (diameter 50 nm) with a concentration of 25 mg·$mL^{-1}$, the increase in temperature is rather fast, with a temperature of 90 °C being achieved in 1 h. In the control experiments, heating of the sample without magnetic nanoparticles was found to be negligible. To avoid higher temperatures, the maximal concentration of magnetic nanoparticles used in all experiments was 2 mg·$mL^{-1}$.

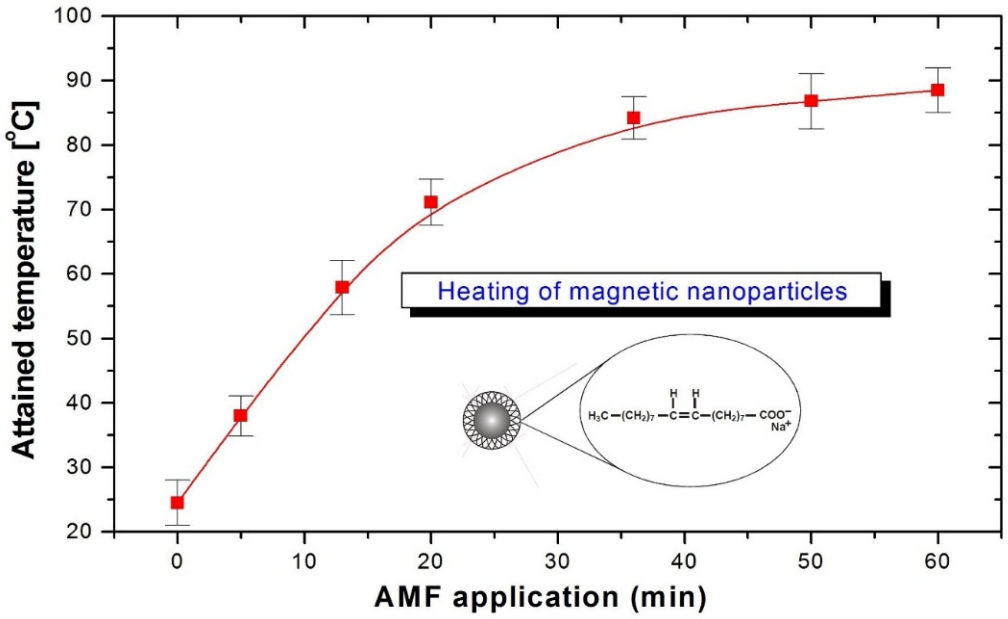



**Figure 5.** Kinetics of the temperature increase of fluidMAG-OS magnetite nanoparticles in 3.5 MHz AMF. Mean values (red squares) and standard deviations (error bars) from five independent experiments.

From measurements of the time-dependent temperature curves, the temperature-to-time variation for the start of heating ($\Delta T/\Delta t$) was calculated from the regression line. For thermally equilibrated samples with steady temperatures before exposure to an AMF-specific loss power (*SLP*), an important parameter characterizing the heating capabilities of magnetic nanoparticles was calculated by the following formula [61]:

$$SLP = C \cdot \frac{m_{sample}}{m_{NP}} \frac{dT}{dt}$$

where *C* is the specific heat capacity of the sample, $m_{NP}$ is the total mass of magnetic nanoparticles in the suspension, $m_{sample}$ is the mass of the sample mixture, *T* is the temperature, and *t* is time. From the measured values, for fluidMA-OS we obtained SAR = 124 W/g at a frequency of 3.5 MHz and a magnetic field of 1.2 kA/m.

The MN's ability to destroy amyloid fibrils is already known [29–33] and is most likely caused by a specific interaction with the hydrophobic groups of the fibrils [62–65]. However, the incubation of nanoparticles with fibrils for several days is then necessary. Such an approach would not be very suitable for removing cutaneous fibril deposits. Therefore, in this work, we tested the possibility of the rapid disintegration of amyloid fibrils if the

application of nanoparticles is combined with the simultaneous action of AMF. For this, we first used fluorescence microscopy, with the help of which we could directly monitor the size of amyloid fibrils formed from HEWL and their size change after the application of different concentrations of nanoparticles under the action of the AMF. ThT-stained individual amyloid fibrils can be viewed using fluorescence microscopy because bounded ThT emits yellow fluorescence under excitation at 450 nm. A reduction in fluorescence intensity with increasing concentration of magnetic nanoparticles was observed (Figure 6), indicating the dissolution of fibrillar species into smaller aggregates due to increased heating after the application of AMF for 15 min.

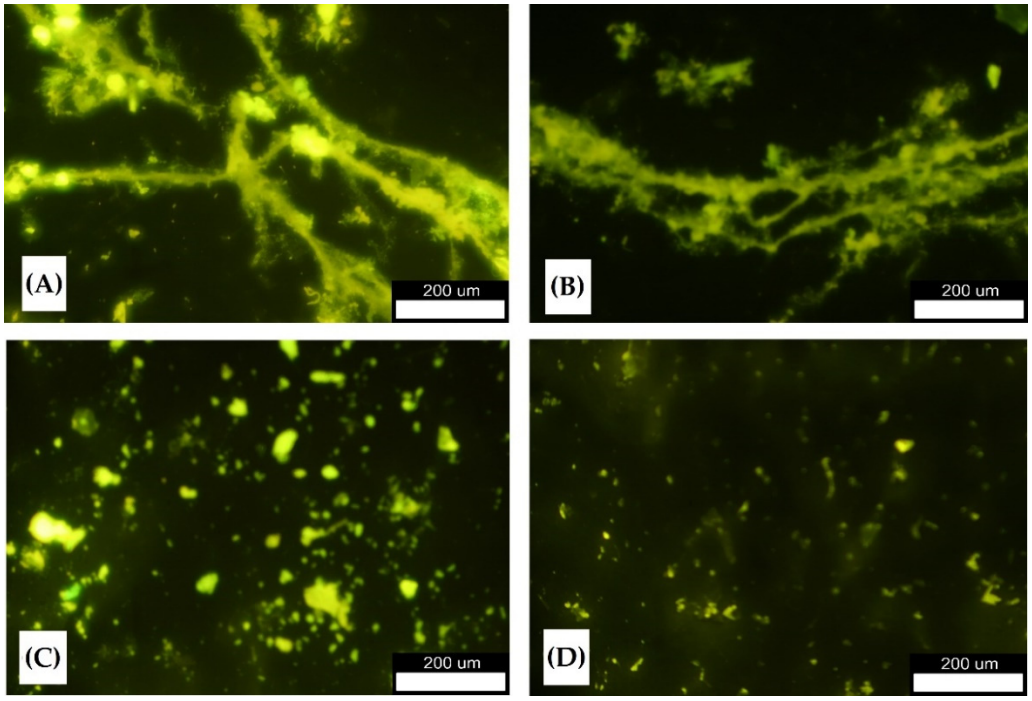



**Figure 6.** Representative images of lysozyme fibrils produced by ThT staining under the fluorescence microscope after the application of AMF for 15 min: (**A**) pure preformed fibrils without MN, (**B**) fibrils with 0.5 mg/mL of MN, (**C**) fibrils with 0.9 mg/mL of MN, and (**D**) fibrils with 1.3 mg/mL of MN. Scale bars: 200 μm.

The UV/Vis spectra for fibrils stained with the *CR* dye are shown in Figure 7. For an approximate quantification of fibrillation, we used two wavelengths corresponding to the *CR* absorption maximum (at 538 nm) observed when it is associated with β plate structures, and to the *CR* absorption peak at (505 nm) when the dye was in its free state in solution [66,67].

$$Relative\ number\ of\ fibrils = \frac{R_X - R_{CR}}{R_{Control} - R_{CR}} \times 100\ (\%)$$

where ratio $R$ is given by

$$R = \frac{ABS_{538}}{ABS_{505}}$$

where subscript X corresponds to the sample of fibrils with concentration X of magnetic nanoparticles after 15 min of AMF application; *CR* corresponds to the sample containing only Congo red; and Control corresponds to initial untreated fibrils saturated by bounded Congo red without magnetic nanoparticles and without the application of an AMF. We found that fluidMAG-OS MN with a concentration greater than 1 mg/mL can almost destroy HEWL fibrils after 15 min of exposure to the AMF field (Figure 8).

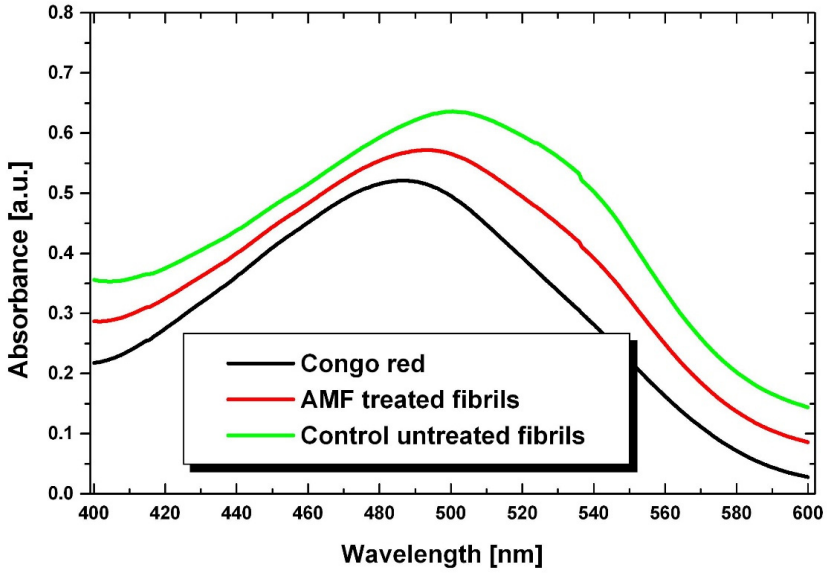



**Figure 7.** Absorbance of fibrils stained with Congo red. AMF-treated fibrils corresponding to the presence of 0.9 mg/mL of magnetic nanoparticles.

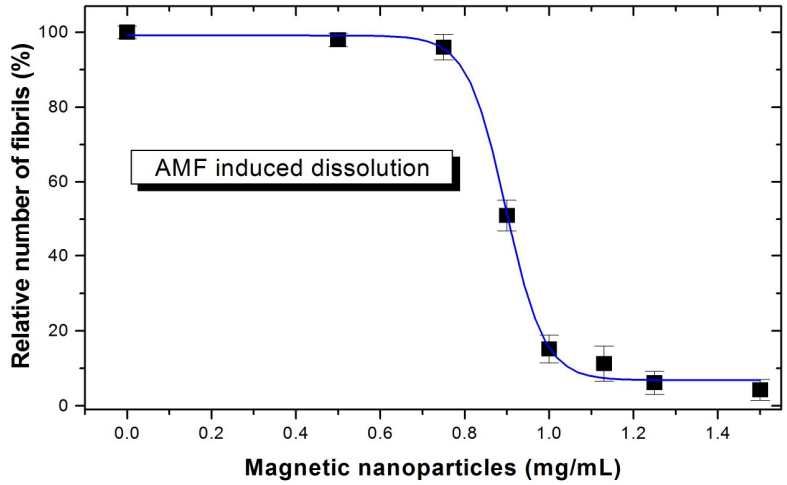


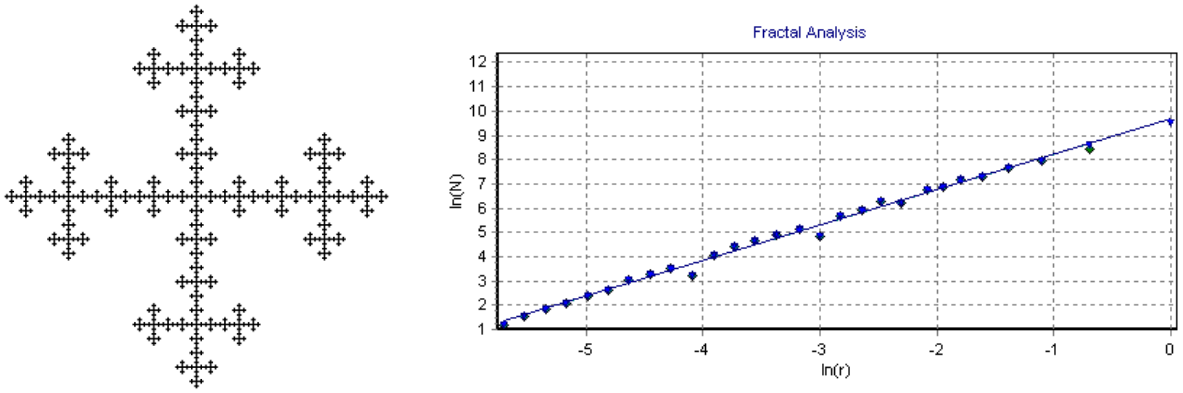

**Figure 8.** Relative number of fibrils after 15 min of applying an alternating magnetic field as a function of MN concentration. On the graph, rescaled values are presented for clarity, where 0% corresponds to pure CR and 100% corresponds to amyloid fibrils without nanoparticles and without the application of a magnetic field. Mean values and standard deviations from three independent experiments.

It should be stressed that the application of AMF without MN does not dissolve preformed fibrils, and MN without AMF application also do not alter them at the studied timescale up to one hour. A 15 min application of MN with an applied AMF is also optimal a therapeutic aspect. In addition, MN can be used for the magnetophoretic extraction of dissolved fibrils from skin lesions [68].

Although in the work we only present the results obtained using fluidMAG-OS, we tested several versions of magnetic nanoparticles with different functionalization provided to us by the company Chemicell GmbH, e.g., starch-functionalized nanoparticles, fluidMAG-D, or poly(maleic acid-co-olefin)-functionalized nanoparticles, fluidMAG-PMO, widely used for purification or separation of biomolecules, as well as for hyperthermia. However, functionalization using sodium oleate proved to be ideal, most likely because sodium oleate consists of a hydrophobic chain as well as a hydrophilic COOH-Na+ group, which both prevent the aggregation of these nanoparticles and make them soluble in water. It can also bind to hydrophilic groups on the surface of fibrils and interact via hydrophobic

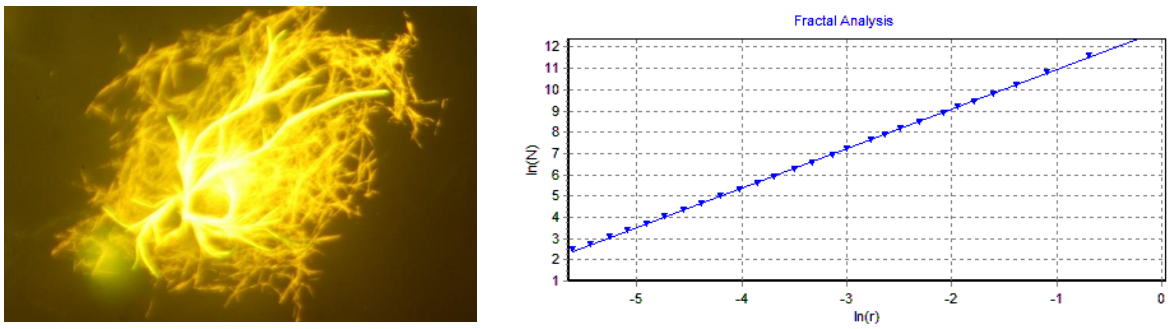
forces, which could be one of the main reasons for the shortening of the amyloids. We believe that fluidMAG-OS nanoparticles with both hydrophobic and hydrophilic properties are unique and promising for amyloid treatment. This effectiveness of sodium oleate is not particularly surprising, since this molecule is a major component of soap as an emulsifying agent. In addition, the heating of MN by AMF can significantly accelerate this process, for example, due to the partial denaturation-induced structure change of HEWL [68,69]. Amyloid fibrils are thermodynamically very stable, and their disruption is extremely difficult. We must emphasize that when using magnetic nanoparticles with a concentration on the order of 1 mg/mL, as we used in the experiments, it was not possible to observe bulk heating; for this effect, 10 times larger concentrations were needed. It is, therefore, localized heating in the vicinity of the nanoparticles which helps and accelerates the process of amyloid dissolution. The detailed mechanism of this process is unknown, but it could be revealed, for example, by molecular simulation at high temperatures [70,71].

In our experiments, we obtained hundreds of photographs of ThT-stained amyloid plaques from a fluorescence microscope; therefore, we decided to also analyze the possible fractal morphology of amyloids. To do so, we used the HarFA v.5.5 program. As can be seen from Figure 9, this program provides very accurate values of fractal dimension D = 1.463 (for comparison, the exact value for this Vicsek fractal is D = log(5)/log(3) = 1.4649). A typical example of fractal analysis of an amyloid fibrillary plaque is shown in Figure 10. The obtained fractal dimension in this case was D = 1.859. By analyzing dozens more structures, we obtained the fractal dimension D = (1.7– 1.9).




(**a**) (**b**)

**Figure 9.** Determination of the fractal dimension: (**a**) Picture of Vicsek fractal; (**b**) Fractal dimension can be calculated as a slope from this linear log-log plot produced by HarFA software: log(N) = 1.463 × log(r).




(**a**) (**b**)

**Figure 10.** Determination of the fractal dimension: (**a**) Picture of lysozyme amyloid plaque; (**b**) Fractal di-mension can be calculated as a slope from this linear log-log plot produced by HarFA software: log(N) = 1.859 × log(r).

The fact that the amyloid plaque is a fractal structure also indicates that the cytotoxicity of amyloids is not a property specific to the morphology of aggregates, but rather an emergent property characterizing the amyloid as a whole [72–74] and it is also reflected by the polymorphism of amyloid fibrils [75]. The observed value of the fractal dimension can be interpreted as a quantitative measure of complexity, characterized by surface irregularities, which are responsible for the interaction with the cellular environment.

A related example is catalysis, where the fractal structure of the catalyst is the most effective because it theoretically has an infinite area per unit mass and, therefore, is best accessible by the reactants.

## 4. Conclusions

Until now, most of the research in amyloid aggregation of proteins has been focused on searching for and testing effective inhibitors. However, in amyloid-related diseases, especially skin-related, amyloid fibrils are already formed between the dermis and epidermis. Therefore, it is equally important to find and investigate the agents which are capable of dissolving the preformed fibrils. The dissolution and clearance of these extremely stable fibrils from lesion is very complicated. We examined the possibility of using magnetic nanoparticles, generating heat in an external alternating magnetic field with a frequency 3.5 MHz, for these purposes. As a convenient model system, we used lysozyme fibrils. For the quantification of fibrillar status we used Thioflavin T as well as Congo red, specific dyes which change their spectroscopic properties upon binding with the cross-beta structure of fibrils. Using fluorescent and polarization microscopy, as well as absorption spectrophotometry, we found that amyloid-like fibrils can be almost completely dissolved. This study, therefore, reveals that the sodium oleate-functionalized magnetic nanoparticles in an alternating magnetic field can efficiently disrupt preformed HEWL fibrillar species.

Radiofrequency (RF) has been used in surgery since the 1920s. In the 1950s, neurosurgeons and cardiac surgeons began to use this method, targeting the burning of unwanted tissues. In the year 2002, the first device was approved by the American FDA (ThermaCool from Thermage, Bothel, USA) to reduce wrinkles and rejuvenate skin, working on the principle of monopolar RF [76]. The first FDA approved device utilizing bipolar RF was Aluma (Lumenis Ltd., Yokneam, Israel). Considering that both monopolar and bipolar RF devices in cosmetic dermatology work most often with a frequency of 1-10 MHz [77,78], our next goal is to test these devices as a sources of AMF for the removal of cutaneous amyloid plaques, using, for example, the intralesional application of magnetic nanoparticles, which is widely used for the application of methotrexate [79]. We hope that our method can be further developed into an effective strategy for the treatment of localized cutaneous amyloidosis, as well as other diseases characterized by insoluble fibrillar deposits in various tissues.

**Author Contributions:** Conceptualization, methodology, validation, formal analysis, investigation, data curation N.A., H.V., P.B., M.B. and M.Š.; Writing—original draft preparation, N.A.; Writing—review and editing, M.B., P.B. and M.Š. All authors have read and agreed to the published version of the manuscript.

**Funding:** This research was funded by the Slovak Grant Agency VEGA project No. 1/0639/22.

**Institutional Review Board Statement:** Not applicable.

**Informed Consent Statement:** Not applicable.

**Data Availability Statement:** Not applicable.

**Conflicts of Interest:** The authors declare no conflict of interest.

## References

1. Šimaljaková, M.; Buchvald, D. *Dermatovenereology*; Comenius University Press: Bratislava, Slovakia, 2019.
2. Chiti, F.; Dobson, C.M. Protein Misfolding, Functional Amyloid, and Human Disease. *Annu. Rev. Biochem.* **2006**, *75*, 333–366. [CrossRef] [PubMed]

3. Fowler, D.M.; Koulov, A.V.; Alory-Jost, C.; Marks, M.; E Balch, W.; Kelly, J.W. Functional Amyloid Formation within Mammalian Tissue. *PLOS Biol.* **2005**, *4*, e6. [CrossRef] [PubMed]
4. Ma, C.; Hong, F.; Yang, S. Amyloidosis in Alzheimer's Disease: Pathogeny, Etiology, and Related Therapeutic Directions. *Molecules* **2022**, *27*, 1210. [CrossRef] [PubMed]
5. Wechalekar, A.D.; Gillmore, J.D.; Hawkins, P.N. Systemic amyloidosis. *Lancet* **2015**, *387*, 2641–2654. [CrossRef]
6. Dogan, A. Amyloidosis: Insights from Proteomics. *Annu. Rev. Pathol. Mech. Dis.* **2017**, *12*, 277–304. [CrossRef]
7. Picken, M.M. The Pathology of Amyloidosis in Classification: A Review. *Acta Haematol.* **2020**, *143*, 322–334. [CrossRef]
8. Hazenberg, B.P. Amyloidosis: A clinical overview. *Rheum. Dis. Clin. N. Am.* **2013**, *39*, 323–345. [CrossRef]
9. Alraawi, Z.; Banerjee, N.; Mohanty, S.; Kumar, T.K.S. Amyloidogenesis: What Do We Know So Far? *Int. J. Mol. Sci.* **2022**, *23*, 13970. [CrossRef]
10. Hamie, L.; Haddad, I.; Nasser, N.; Kurban, M.; Abbas, O. Primary Localized Cutaneous Amyloidosis of Keratinocyte Origin: An Update with Emphasis on Atypical Clinical Variants. *Am. J. Clin. Dermatol.* **2021**, *22*, 667–680. [CrossRef]
11. Low, K.J.Y.; Venkatraman, A.; Mehta, J.S.; Pervushin, K. Molecular mechanisms of amyloid disaggregation. *J. Adv. Res.* **2021**, *36*, 113–132. [CrossRef]
12. Almeida, Z.L.; Brito, R.M.M. Amyloid Disassembly: What Can We Learn from Chaperones? *Biomedicines* **2022**, *10*, 3276. [CrossRef]
13. Almeida, Z.L.; Brito, R.M.M. Structure and Aggregation Mechanisms in Amyloids. *Molecules* **2020**, *25*, 1195. [CrossRef]
14. Picone, P.; Sanfilippo, T.; Vasto, S.; Baldassano, S.; Guggino, R.; Nuzzo, D.; Bulone, D.; Biagio, P.L.S.; Muscolino, E.; Monastero, R.; et al. From Small Peptides to Large Proteins against Alzheimer'sDisease. *Biomolecules* **2022**, *12*, 1344. [CrossRef]
15. Shao, X.; Yan, C.; Wang, C.; Cao, Y.; Zhou, Y.; Guan, P.; Hu, X.; Zhu, W.; Ding, S. Advanced nanomaterials for modulating Alzheimer's related amyloid aggregation. *Nanoscale Adv.* **2022**, *5*, 46–80. [CrossRef]
16. Liang, C.-Q.; Li, Y.-M. Peptides for disrupting and degrading amyloids. *Curr. Opin. Chem. Biol.* **2021**, *64*, 124–130. [CrossRef]
17. Huang, Y.; Chang, Y.; Liu, L.; Wang, J. Nanomaterials for Modulating the Aggregation of β-Amyloid Peptides. *Molecules* **2021**, *26*, 4301. [CrossRef]
18. Andrei, M.; Wang, J.C. Cutaneous light chain amyloidosis with multiple myeloma: A concise review. *Hematol. Stem Cell Ther.* **2018**, *12*, 71–81. [CrossRef]
19. Wenson, S.F.; Jessup, C.J.; Johnson, M.M.; Cohen, L.M.; Mahmoodi, M. Primary cutaneous amyloidosis of the external ear: A clinicopathological and immunohistochemical study of 17 cases. *J. Cutan. Pathol.* **2011**, *39*, 263–269. [CrossRef]
20. Fernandez-Flores, A. Cutaneous Amyloidosis: A Concept Review. *Am. J. Dermatopathol.* **2012**, *34*, 1–17. [CrossRef]
21. Schreml, S.; Szeimies, R.-M.; Vogt, T.; Landthaler, M.; Schroeder, J.; Babilas, P. Cutaneous amyloidoses and systemic amyloidoses with cutaneous involvement. *Eur. J. Dermatol.* **2010**, *20*, 152–160. [CrossRef]
22. Yoneyama, K.; Tochigi, N.; Oikawa, A.; Shinkai, H.; Utani, A. Primary Localized Cutaneous Nodular Amyloidosis in a Patient with Sjögren's Syndrome: A Review of the Literature. *J. Dermatol.* **2005**, *32*, 120–123. [CrossRef] [PubMed]
23. Weidner, T.; Illing, T.; Elsner, P. Primary Localized Cutaneous Amyloidosis: A Systematic Treatment Review. *Am. J. Clin. Dermatol.* **2017**, *18*, 629–642. [CrossRef] [PubMed]
24. Ahramiyanpour, N.; Akbari, Z.; Sarasyabi, M.S.; Aflatoonian, M.; Saki, N.; Shafie'ei, M. The therapeutic role of lasers in pri-mary localized cutaneous amyloidosis: A systematic review. *Lasers Med. Sci.* **2022**, *37*, 799–813. [CrossRef] [PubMed]
25. Swaminathan, R.; Ravi, V.K.; Kumar, S.; Kumar, M.V.S.; Chandra, N. Lysozyme. *Rev. Med. Interne.* **2011**, *84*, 63–111. [CrossRef]
26. Scafi, M.; Valleix, S.; Benyamine, A.; Jean, E.; Harlé, J.-R.; Rossi, P.; Daniel, L.; Schleinitz, N.; Granel, B. L'amylose à lysozyme: A model protein for amyloid research. *Adv. Protein Chem. Struct. Biol.* **2018**, *40*, 323–329. [CrossRef]
27. Pleyer, C.; Flesche, J.; Saeed, F. Lysozyme amyloidosis–A case report and review of the literature. *Clin. Nephrol. Case Stud.* **2015**, *3*, 42–45. [CrossRef]
28. Booth, D.R.; Sunde, M.; Bellotti, V.; Robinson, C.V.; Hutchinson, W.L.; Fraser, P.E.; Hawkins, P.N.; Dobson, C.M.; Radford, S.E.; Blake, C.C.; et al. Instability, unfolding and aggregation of human lysozyme variants underlying amyloid fibrillogenesis. *Nature* **1997**, *385*, 787–793. [CrossRef]
29. Gombos, J.; Balejcikova, L.; Kopcansky, P.; Batkova, M.; Siposova, K.; Kovac, J.; Zolochevska, K.; Safarik, I.; Lokajova, A.; Garamus, V.M.; et al. Destruction of Lysozyme Amyloid Fibrils Induced by Magnetoferritin and Reconstructed Ferritin. *Int. J. Mol. Sci.* **2022**, *23*, 13926. [CrossRef]
30. Bellova, A.; Bystrenova, E.; Koneracka, M.; Kopcansky, P.; Valle, F.; Tomasovicova, N.; Timko, M.; Bagelova, J.; Biscarini, F.; Gazova, Z. Effect of $Fe_3O_4$ magnetic nanoparticles on lysozyme amyloid aggregation. *Nanotechnology* **2010**, *21*, 065103. [CrossRef]
31. Solin, N. Amyloid-like fibrils labeled with magnetic nanoparticles. *Biomol. Concepts* **2013**, *4*, 425–432. [CrossRef]
32. Majorosova, J.; Petrenko, V.I.; Siposova, K.; Timko, M.; Tomasovicova, N.; Garamus, V.M.; Koralewski, M.; Avdeev, M.V.; Leszczynski, B.; Jurga, S.; et al. On the adsorption of magnetite nanoparticles on lysozyme amyloid fibrils. *Colloids Surfaces B Biointerfaces* **2016**, *146*, 794–800. [CrossRef]
33. Antosova, A.; Gancar, M.; Bednarikova, Z.; Marek, J.; Zahn, D.; Dutz, S.; Gazova, Z. Surface-modified magnetite nanoparticles affect lysozyme amyloid fibrillization. *Biochim. et Biophys. Acta BBA Gen. Subj.* **2021**, *1865*, 129941. [CrossRef]
34. Lee, W.; Jung, H.; Son, M.; Lee, H.; Kwak, T.J.; Lee, G.; Kim, C.H.; Lee, S.W.; Yoon, D.S. Characterization of the regrowth behavior of amyloid-like fragmented fibrils decomposed by ultrasonic treatment. *RSC Adv.* **2014**, *4*, 56561–56566. [CrossRef]

35. Loynachan, C.N.; Romero, G.; Christiansen, M.G.; Chen, R.; Ellison, R.; O'Malley, T.T.; Froriep, U.P.; Walsh, D.M.; Anikeeva, P. Targeted Magnetic Nanoparticles for Remote Magnetothermal Disruption of Amyloid-β Aggregates. *Adv. Health Mater.* **2015**, *4*, 2100–2109. [CrossRef]
36. Dyne, E.; Prakash, P.S.; Li, J.; Yu, B.; Schmidt, T.-L.; Huang, S.; Kim, M.-H. Mild magnetic nanoparticle hyperthermia promotes the disaggregation and microglia-mediated clearance of beta-amyloid plaques. *Nanomed. Nanotechnol. Biol. Med.* **2021**, *34*, 102397. [CrossRef]
37. Bastús, N.G.; Kogan, M.J.; Amigo, R.; Grillo-Bosch, D.; Araya, E.; Turiel, A.; Labarta, A.; Giralt, E.; Puntes, V.F. Gold nanoparticles for selective and remote heating of β-amyloid protein aggregates. *Mater. Sci. Eng. C* **2007**, *27*, 1236–1240. [CrossRef]
38. Triulzi, R.C.; Dai, Q.; Zou, J.; Leblanc, R.M.; Gu, Q.; Orbulescu, J.; Huo, Q. Photothermal ablation of amyloid aggregates by gold nanoparticles. *Colloids Surf. B Biointerfaces* **2008**, *63*, 200–208. [CrossRef]
39. Babincová, M. Microwave induced likage of magnetoliposomes. Possible clinical implications. *Bioelectrochem. Bioenerg.* **1993**, *32*, 187–189. [CrossRef]
40. Babincová, M.; Vrbovská, H.; Sourivong, P.; Babinec, P.; Durdík, Š. Application of Albumin-embedded Magnetic Nanoheaters for Release of Etoposide in Integrated Chemotherapy and Hyperthermia of U87-MG Glioma Cells. *Anticancer. Res.* **2018**, *38*, 2683–2690. [CrossRef]
41. Caizer, C. Optimization Study on Specific Loss Power in Superparamagnetic Hyperthermia with Magnetite Nanoparticles for High Efficiency in Alternative Cancer Therapy. *Nanomaterials* **2020**, *11*, 40. [CrossRef]
42. Zahn, D.; Landers, J.; Buchwald, J.; Diegel, M.; Salamon, S.; Müller, R.; Köhler, M.; Ecke, G.; Wende, H.; Dutz, S. Ferrimagnetic Large Single Domain Iron Oxide Nanoparticles for Hyperthermia Applications. *Nanomaterials* **2022**, *12*, 343. [CrossRef] [PubMed]
43. Dutz, S.; Hergt, R. Magnetic particle hyperthermia—A promising tumour therapy? *Nanotechnology* **2014**, *25*, 452001. [CrossRef] [PubMed]
44. Dutz, S.; Hergt, R. Magnetic nanoparticle heating and heat transfer on a microscale: Basic principles, realities and physical limitations of hyperthermia for tumour therapy. *Int. J. Hyperth.* **2013**, *29*, 790–800. [CrossRef]
45. Babincová, N.; Sourivong, P.; Babinec, P.; Bergemann, C.; Babincová, M.; Durdík, S. Applications of magnetoliposomes with encapsulated doxorubicin for integrated chemotherapy and hyperthermia of rat C6 glioma. *Z. Nat. C* **2018**, *73*, 265–271. [CrossRef] [PubMed]
46. Altanerova, U.; Babincova, M.; Babinec, P.; Benejova, K.; Jakubechova, J.; Altanerova, V.; Zduriencikova, M.; Repiska, V.; Altaner, C. Human mesenchymal stem cell-derived iron oxide exosomes allow targeted ablation of tumor cells via magnetic hyperthermia. *Int. J. Nanomed.* **2017**, *12*, 7923–7936. [CrossRef]
47. Myers, J.K. Spectroscopic Characterization of Amyloid Fibril Formation by Lysozyme. *J. Chem. Educ.* **2014**, *91*, 730–733. [CrossRef]
48. Yakupova, E.I.; Bobyleva, L.G.; Vikhlyantsev, I.M.; Bobylev, A.G. Congo Red and amyloids: History and relationship. *Biosci. Rep.* **2019**, *39*, 1495–1506. [CrossRef]
49. Howie, A.J. "Green (or apple-green) birefringence" of Congo red-stained amyloid. *Amyloid* **2015**, *22*, 205–206. [CrossRef]
50. Howie, A.J.; Brewer, D.B. Optical properties of amyloid stained by Congo red: History and mechanisms. *Micron* **2008**, *40*, 285–301. [CrossRef]
51. Howie, A.J.; Brewer, D.B.; Howell, D.; Jones, A.P. Physical basis of colors seen in Congo red-stained amyloid in polarized light. *Lab. Investig.* **2008**, *88*, 232–242. [CrossRef]
52. Zmeskal, O.; Bzatek, T.; Nezadal, M.; HarFA: Harmonic and Fractal Image Analyser. Software for Determination of Fractal Dimension. Available online: http://www.fch.vutbr.cz/lectures/imagesci (accessed on 19 March 2017).
53. Yang, K.; Peng, H.; Wen, Y.; Li, N. Re-examination of characteristic FTIR spectrum of secondary layer in bilayer oleic acid-coated Fe3O4 nanoparticles. *Appl. Surf. Sci.* **2009**, *256*, 3093–3097. [CrossRef]
54. Tombácz, E.; Bica, D.; Hajdú, A.; Illés, E.; Majzik, A.; Vékás, L. Surfactant double layer stabilized magnetic nanofluids for bio-medical application. *J. Phys. Condens. Matter* **2008**, *20*, 204103. [CrossRef]
55. Jiang, W.; Wu, Y.; He, B.; Zeng, X.; Lai, K.; Gu, Z. Effect of sodium oleate as a buffer on the synthesis of superparamagnetic magnetite colloids. *J. Colloid Interface Sci.* **2010**, *347*, 1–7. [CrossRef]
56. Bateer, B.; Qu, Y.; Meng, X.; Tian, C.; Du, S.; Wang, R.; Pan, K.; Fu, H. Preparation and magnetic performance of the magnetic fluid stabilized by bi-surfactant. *J. Magn. Magn. Mater.* **2012**, *332*, 151–156. [CrossRef]
57. Sun, J.; Zhou, S.; Hou, P.; Yang, Y.; Weng, J.; Li, X.; Li, M. Synthesis and characterization of biocompatible Fe3O4 nanoparticles. *J. Biomed. Mater. Res. Part A* **2006**, *80A*, 333–341. [CrossRef]
58. Jain, T.K.; Reddy, M.K.; Morales, M.A.; Leslie-Pelecky, D.L.; Labhasetwar, V. Biodistribution, Clearance, and Biocompatibility of Iron Oxide Magnetic Nanoparticles in Rats. *Mol. Pharm.* **2008**, *5*, 316–327. [CrossRef]
59. Atkinson, W.J.; Brezovich, I.A.; Chakraborty, D.P. Usable Frequencies in Hyperthermia with Thermal Seeds. *IEEE Trans. Biomed. Eng.* **1984**, *BME-31*, 70–75. [CrossRef]
60. Hergt, R.; Dutz, S. Magnetic particle hyperthermia—Biophysical limitations of a visionary tumour therapy. *J. Magn. Magn. Mater.* **2007**, *311*, 187–192. [CrossRef]
61. Garaio, E.; Sandre, O.; Collantes, J.-M.; Garcia, J.A.; Mornet, S.; Plazaola, F. Specific absorption rate dependence on temperature in magnetic field hyperthermia measured by dynamic hysteresis losses (ac magnetometry). *Nanotechnology* **2014**, *26*, 015704. [CrossRef]

62. Makshakova, O.; Bogdanova, L.; Faizullin, D.; Khaibrakhmanova, D.; Ziganshina, S.; Ermakova, E.; Zuev, Y.; Sedov, I. The Ability of Some Polysaccharides to Disaggregate Lysozyme Amyloid Fibrils and Renature the Protein. *Pharmaceutics* **2023**, *15*, 624. [CrossRef]
63. Capocefalo, A.; Deckert-Gaudig, T.; Brasili, F.; Postorino, P.; Deckert, V. Unveiling the interaction of protein fibrils with gold nanoparticles by plasmon enhanced nano-spectroscopy. *Nanoscale* **2021**, *13*, 14469–14479. [CrossRef] [PubMed]
64. Barbalinardo, M.; Antosova, A.; Gambucci, M.; Bednarikova, Z.; Albonetti, C.; Valle, F.; Sassi, P.; Latterini, L.; Gazova, Z.; Bystrenova, E. Effect of metallic nanoparticles on amyloid fibrils and their influence to neural cell toxicity. *Nano Res.* **2020**, *13*, 1081–1089. [CrossRef]
65. Ban, D.K.; Paul, S. Functionalized gold and silver nanoparticles modulate amyloid fibrillation, defibrillation and cytotoxicity of lysozyme via altering protein surface character. *Appl. Surf. Sci.* **2018**, *473*, 373–385. [CrossRef]
66. Mari, E.; Ricci, C.; Pieraccini, S.; Spinozzi, F.; Mariani, P.; Ortore, M.G. Trehalose Effect on The Aggregation of Model Proteins into Amyloid Fibrils. *Life* **2020**, *10*, 60. [CrossRef]
67. Mastrella, L.; Moretti, P.; Pieraccini, S.; Magi, S.; Piccirillo, S.; Ortore, M.G. Taurine Stabilizing Effect on Lysozyme. *Life* **2022**, *12*, 133. [CrossRef]
68. Skaat, H.; Sorci, M.; Belfort, G.; Margel, S. Effect of maghemite nanoparticles on insulin amyloid fibril formation: Selective labeling, kinetics, and fibril removal by a magnetic field. *J. Biomed. Mater. Res. Part A* **2008**, *91A*, 342–351. [CrossRef]
69. Fitzpatrick, A.W.P.; Debelouchina, G.T.; Bayro, M.J.; Clare, D.K.; Caporini, M.A.; Bajaj, V.S.; Jaroniec, C.P.; Wang, L.; Ladizhansky, V.; Müller, S.A.; et al. Atomic structure and hierarchical assembly of a cross-β amyloid fibril. *Proc. Natl. Acad. Sci. USA* **2013**, *110*, 5468–5473. [CrossRef]
70. Perutz, M.F. Amyloid fibrils. Mutations make enzyme polymerize. *Nature* **1997**, *385*, 773. [CrossRef]
71. Fitzpatrick, A.W.P.; Vanacore, G.M.; Zewail, A.H. Nanomechanics and intermolecular forces of amyloid revealed by four-dimensional electron microscopy. *Proc. Natl. Acad. Sci. USA* **2015**, *112*, 3380–3385. [CrossRef]
72. Bucciantini, M.; Rigacci, S.; Stefani, M. Amyloid Aggregation: Role of Biological Membranes and the Aggregate–Membrane System. *J. Phys. Chem. Lett.* **2014**, *5*, 517–527. [CrossRef]
73. Gillet, J.N. From molecular dynamics to quantum mechanics of misfolded proteins and amyloid-like macroaggregates applied to neurodegenerative diseases. *J. Mol. Graph. Model.* **2022**, *112*, 108046. [CrossRef]
74. Come, J.H.; E Fraser, P.; Lansbury, P.T. A kinetic model for amyloid formation in the prion diseases: Importance of seeding. *Proc. Natl. Acad. Sci. USA* **1993**, *90*, 5959–5963. [CrossRef]
75. Mocanu, M.-M.; Ganea, C.; Siposova, K.; Filippi, A.; Demjen, E.; Marek, J.; Bednarikova, Z.; Antosova, A.; Baran, I.; Gazova, Z. Polymorphism of hen egg white lysozyme amyloid fibrils influences the cytotoxicity in LLC-PK1 epithelial kidney cells. *Int. J. Biol. Macromol.* **2014**, *65*, 176–187. [CrossRef] [PubMed]
76. Beasley, K.L.; Weiss, R.A. Radiofrequency in Cosmetic Dermatology. *Dermatol. Clin.* **2014**, *32*, 79–90. [CrossRef]
77. Suh, D.H.; Ahn, H.; Seo, J.; Lee, S.J.; Shin, M.K.; Song, K.Y. Monopolar radiofrequency treatment for facial laxity: Histometric analysis. *J. Cosmet. Dermatol.* **2020**, *19*, 2317–2324. [CrossRef]
78. Sadick, N.S.; Nassar, A.H.; Dorizas, A.S.; Alexiades-Armenakas, M. Bipolar and Multipolar Radiofrequency. *Dermatol. Surg.* **2014**, *40*, S174–S179. [CrossRef]
79. Searle, T.; Ali, F.R.; Al-Niaimi, F. Intralesional methotrexate in dermatology: Diverse indications and practical considerations. *Dermatol. Ther.* **2020**, *34*, e14404. [CrossRef]


**Disclaimer/Publisher's Note:** The statements, opinions and data contained in all publications are solely those of the individual author(s) and contributor(s) and not of MDPI and/or the editor(s). MDPI and/or the editor(s) disclaim responsibility for any injury to people or property resulting from any ideas, methods, instructions or products referred to in the content.